



Brigham Young University
Department of Electrical and
Computer Engineering
Microwave Earth Remote
Sensing (MERS) Laboratory



459 Clyde Building
Provo, Utah 84602

Estimating the ASCAT Spatial Response Function

Richard D. Lindsley

May 22, 2014

Revised 5 Jan 2015

www.mers.byu.edu

MERS Technical Report # MERS 14-01

Microwave Earth Remote Sensing (MERS)
Laboratory

Estimating the ASCAT Spatial Response Function

Richard D. Lindsley

May 22, 2014; revised Jan 5, 2015

Abstract

The spatial response function (SRF) for ASCAT is required for land fraction computation and enhanced resolution image reconstruction. In this report we develop an estimate of the SRF. The estimate includes the nominal antenna response, the frequency response of the FFT bins, along-track pulse averaging, and rotation induced by Doppler.

To speed up SRF computation, a parameterized SRF is also developed. This models the SRF as separable in orthogonal components, with the response in each direction modeled by a polynomial response. This approximation is two orders of magnitude faster to compute and the approximation error is negligible for the required SRF applications.

1 Introduction

The ASCAT spatial response function (SRF) is computed in the ASCAT ground processing to develop the raw data to a level 1B product. However, the SRF is also required after L1B processing in order to compute the measurement land fraction or to enable enhanced resolution processing. This motivates developing an estimate of the SRF that uses only L1B quantities (reported measurement center, incidence angle, etc) rather than raw quantities (reported ground and slant range, orbit state vectors, etc).

This report develops an estimate of the SRF based on L1B inputs. The estimate includes the antenna response, the response due to the on-board FFT processing, and the along-track pulse averaging. Additionally, a parameterized SRF estimate is developed that models the SRF rather than fully computing it for each measurement. This parameterized estimate is much faster to compute than the full estimate and is preferred for enhanced resolution processing at the MERS Lab. A background on ASCAT and its on-board processing is presented in Section 2. The full SRF estimate is developed in Section 3 and the parameterized version in Section 4. Some examples and comparisons of the resulting SRF estimates are illustrated in Section 5. Section 6 concludes.

2 Background

ASCAT (Advanced Scatterometer) is a C-band fan beam scatterometer [1]. An ASCAT is hosted on each of the MetOp satellites. MetOp-A launched in 2006, MetOp-B in 2012,

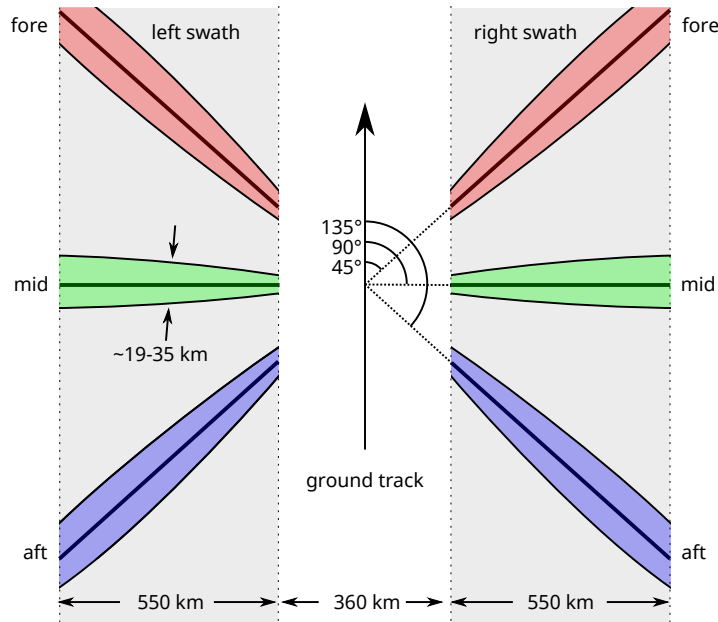


Figure 1: The ASCAT ground geometry. Each swath is sampled at a range of incidence angles at azimuth angles fore, mid, and aft. Antenna beamwidth is exaggerated for illustrative purposes.

and MetOp-C is scheduled for 2018.

ASCAT has two swaths, one on each side, with three beams in each swath. The beams are aligned in fore, mid, and aft azimuth angles. The ground geometry is shown in Fig. 1. Range-Doppler processing subdivides each beam into 256 locations, although only 192 of these values are reported in the current data format [2].

The measurement values (radar backscatter, incidence angle, azimuth angle) and location (in latitude and longitude) are reported for each measurement node for each beam. This is the “full resolution” (SZF) L1B product. Spatially averaged products (SZO, SZR) are also produced where a swath-oriented grid is defined and the value at each grid point is the combination of all nearby full-resolution measurements, spatially weighted with a Hamming window. This report does not consider the spatially averaged products.

The measurement spatial response function (SRF) or measurement footprint is the weighting each location on the Earth surface contributes to the measurement:

$$z_i = \iint \sigma^\circ(x, y) h_i(x, y) dx dy \quad (1)$$

where z_i is the noise-free measurement, $\sigma^\circ(x, y)$ the true Earth surface radar backscatter, and $h_i(x, y)$ the SRF associated with measurement z_i . The SRF is effectively a function of the antenna pattern and the on-board processing. The nominal beam antenna patterns are shown in Fig. 2. The on-board processing has two major components: the range-Doppler processing, discussed in Section 2.1, and the along-track pulse averaging, discussed in Section 2.2.

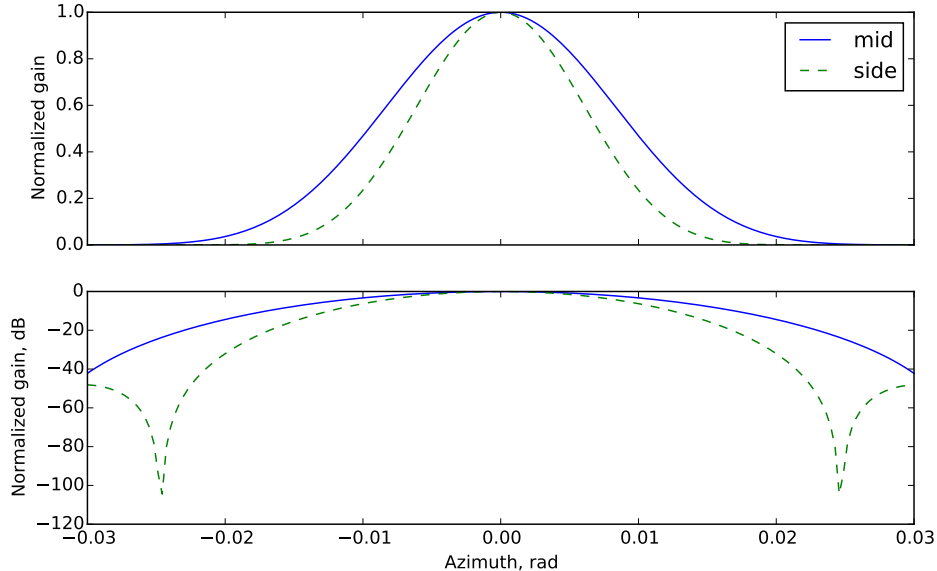


Figure 2: The cross-beam or azimuthal nominal antenna patterns. The mid (solid) and side (dashed) beams are shown together. The upper subplot is in linear space, the lower subplot in dB space. The values shown are for the magnitude-squared normalized antenna gain pattern.

2.1 Range-Doppler processing

ASCAT is a pulsed radar, with each pulse a linear FM chirp. The received signal—multiple time-delayed and attenuated copies of the transmit chirp—is dechirped to baseband. This baseband signal is also termed the *discriminator signal* and is sampled at 412.5 kHz. The power spectrum of the discriminator signal is estimated using Welch’s method (multiple overlapping segments of the sampled time-domain data are taken, separately FFT-ed, magnitude-squared, then averaged together). Each overlapping segment is termed a *range look*, and a 512-point FFT is used [3]. We denote the discretely sampled power spectrum estimate here as $P[f]$.

The center frequency of each discriminator frequency FFT bin is given by [3]

$$f_{\text{offset}} - \underbrace{\frac{4\alpha s}{c}}_{f_r} - \underbrace{\frac{2v_r}{\lambda}}_{f_d} = i\delta_f \quad (2)$$

where f_{offset} is a beam-dependent frequency offset, α is the beam-dependent chirp rate, s the slant range from ASCAT to the Earth surface, c the speed of light, v_r the radial velocity between ASCAT and the Earth surface, λ the radar wavelength, i the FFT bin number, and δ_f the frequency bin width. Values for some of these parameters are given in Table 1.

Equation (2) is solved for slant range s to map power as a function of frequency to power as a function of slant range. Using the radar equation, power is normalized to σ° , so that $P[f]$ transforms to $\sigma^\circ[s]$. With a known slant range and antenna azimuth angle, the σ° measurements are geolocated on the Earth reference ellipsoid.

Table 1: Discriminator frequency parameters for Eq. (2).

| Term | Value |
|----------------------------------|--|
| $f_{\text{offset}}(\text{fore})$ | $-189.0 \times 10^3 \text{ Hz}$ |
| $f_{\text{offset}}(\text{mid})$ | $-286.2 \times 10^3 \text{ Hz}$ |
| $f_{\text{offset}}(\text{aft})$ | $400.6 \times 10^3 \text{ Hz}$ |
| $\alpha(\text{fore})$ | $-1.03 \times 10^7 \text{ Hz/s}$ |
| $\alpha(\text{mid})$ | $-2.69 \times 10^7 \text{ Hz/s}$ |
| $\alpha(\text{aft})$ | $+1.03 \times 10^7 \text{ Hz/s}$ |
| λ | $\frac{c}{f} = 5.71 \text{ cm}$ |
| i | $0, 1, \dots, 255$ |
| δ_f | $\frac{412.5 \text{ kHz}}{512} = 805.7 \text{ Hz}$ |

As noted by the underbraces in Eq. (2), the discriminator frequency has components due to a range frequency, f_r , and a Doppler frequency, f_d . Thus, all locations on the Earth that have (continuous) frequencies $f_{\text{offset}} - (f_r + f_d)$ within an FFT bin¹ contribute to the measurement.

An illustration of how f_r and f_d contribute to the measurement SRF is shown in Fig. 3. Lines of constant range, isoranges, and lines of constant Doppler frequency, isodops, are shown. A zoomed illustration of a mid-looking ASCAT beam is shown in Fig. 4. Isoranges and isodops are again illustrated. Since the discriminator frequency is the combination of f_r and f_d , a line of constant discriminator frequency does not follow an isorange—range and Doppler couple together into the discriminator frequency.

2.2 Along-track pulse averaging

In addition to the range-Doppler processing described above, along-track averaging is performed [4, Appendix]. Each reported measurement is the weighted average of eight pulses. The weights are: $\{0.05, 0.10, 0.15, 0.20, 0.20, 0.15, 0.10, 0.05\}$ and a measurement is saved every four pulses. The radar itself has a pulse repetition frequency (PRF) of approximately 28.26 Hz [5]. This is divided among the six beams, which are pulsed in sequence (left fore, left mid, left aft, right fore, right mid, right aft). Thus the PRF for each beam is $28.26/6 = 4.71 \text{ Hz}$. Every four beam pulses, a row of measurements is saved, so the measurements are stored at a PRF of $4.71/4 = 1.1775 \text{ Hz}$, or about every 5.6 km along-track.

3 Full SRF Estimate

The full SRF estimate is performed on a per-measurement basis with inputs: beam number, incidence angle, azimuth angle, latitude, longitude, ascending/descending pass,

¹More accurately, due to the frequency response of an FFT bin, each FFT bin is the weighted combination of all frequencies. However, the frequency response mainlobe is approximately as wide as the bin edges so for this discussion we are treating the FFT frequency response as a rect with width equal to the bin width.

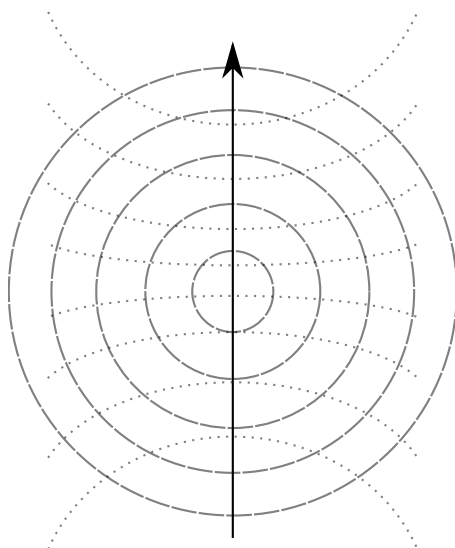


Figure 3: An illustration of lines of constant range, isoranges, and lines of constant Doppler, isodops. Isoranges are circles centered at nadir. Isodops are hyperbolic. The exact isoranges and isodops are complicated by the fact that they are projected on a ellipsoidal Earth. The relative motion between the orbiting satellite and the rotating Earth further complicates the isodops.

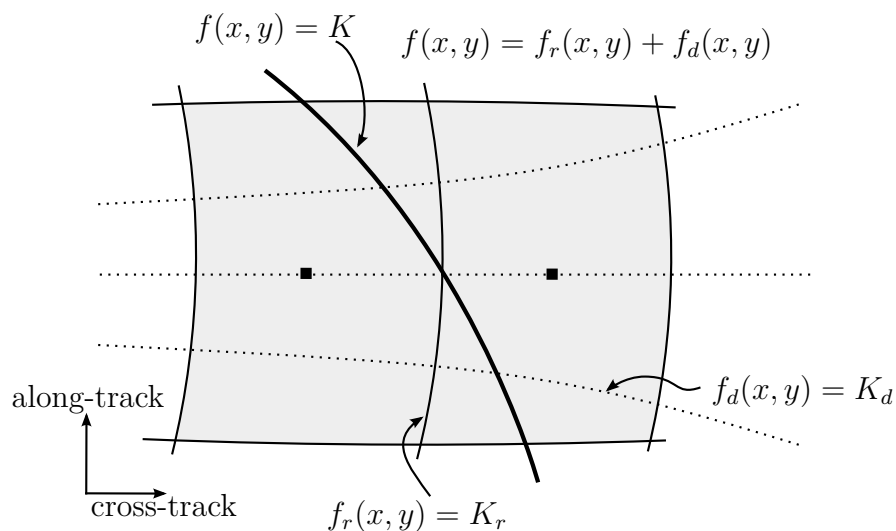


Figure 4: An illustration of a portion from a mid beam. Any point on the ground in (x, y) has a discriminator frequency $f(x, y)$ (ignoring f_{offset}). Isoranges and isodops are plotted, along with measurement centers indicated with the dark squares. A line of constant discriminator frequency is also denoted and is roughly a tilted isorange line.

and node index. These are all reported in the ASCAT L1B data. The measurement SRF is computed on a locally tangent plane centered on the reported location. Details on transforming between latitude/longitude and tangent plane coordinates are found in [6]. Due to the tangent plane breaking down near the poles², measurements with extreme latitudes ($> |89.5^\circ|$) are not used.

We note that the geometry below at times uses an ellipsoidal Earth, following the WGS-84 definition, and at other times a spherical Earth model. A spherical Earth permits simplifying to spherical trigonometry. This approximation error is deemed to be negligible but is non-zero.

First the “pulse SRF” is computed. This is the SRF for a single ASCAT pulse. Due to the on-board pulse averaging, the cumulative response, or “measurement SRF” is the weighted combination of several pulse SRFs. The creation of both SRFs is detailed below.

3.1 Pulse SRF

On the locally tangent plane, we define a grid centered on the measurement. The tangent plane and the grid are aligned with North and East rather than with along-track/cross-track. At each grid point, several quantities are computed:

1. The ground range between the grid point and the nadir location
2. The slant range between the grid point and the satellite
3. The range frequency f_r
4. The ground and slant ranges after a time differential δ_t
5. The radial velocity
6. The Doppler frequency f_d
7. The discriminator signal frequency
8. The distance in antenna azimuth from the center
9. The antenna response value
10. The FFT response value

These quantities are computed below and shown for a sample measurement.

Figure 5 illustrates the geometry. ASCAT is at an altitude h above the nadir point n . The measurement center c has a slant range r and ground range g . Due to the Earth curvature, the local incidence angle θ is not exactly equal to the nadir angle ψ . The ground range lies along the great circle connecting n and c . R_E is the local Earth radius. In order to easily convert between r and g , the local radius R_E is assumed to be the

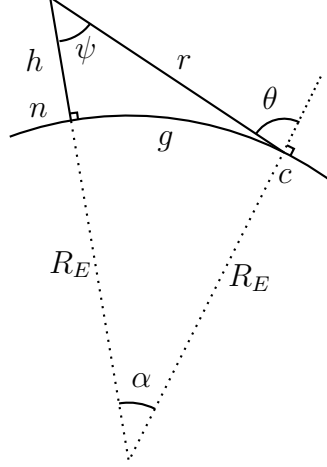


Figure 5: The geometry of the curved Earth model. A spherical Earth is used here. An ellipsoidal model would have slightly different R_E lengths to locations n and c . See text for definitions.

same at n and c , but a marginally more accurate computation models the Earth as an ellipsoid and uses different radii at these locations.

Of these quantities, only the center location c in latitude and longitude and the local incidence angle θ is reported in the L1B data. A nominal altitude of $h = 820$ km is assumed. The local Earth radius is defined as

$$R_E = R_M(1 - \epsilon \sin^2 l), \quad (3)$$

where $R_M = 6378.1363$ km is the mean Earth equatorial radius, $\epsilon = 1/298.257$ is the flattening constant, and l is the reported latitude. The nadir angle ψ is

$$\psi = \sin^{-1} \left[\frac{R_E}{R_{sat}} \sin \theta \right], \quad (4)$$

where $R_{sat} = R_E + h$ is the radius to the satellite. Then the slant range r is

$$r = R_{sat} \left[\cos \psi - \sqrt{\left(\frac{R_E}{R_{sat}} \right)^2 - \sin^2 \psi} \right]. \quad (5)$$

The ground range g may be found either through a great-circle distance between n and c or by first finding the central angle α :

$$\alpha = \sin^{-1} \left[\frac{r}{R_E} \sin \psi \right], \quad (6)$$

and then the arc length is g (with α in radians):

$$g = R_E \alpha. \quad (7)$$

²An `arcsin` with argument > 1 is computed since the requested location “wraps over” the pole. This gives a non-real result.

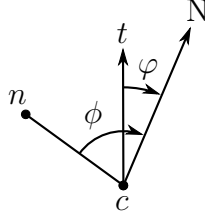


Figure 6: The geometry to find the angles from the ground range line and the track direction to North. This case is for an ascending pass, right aft beam. Here, ϕ is roughly -60° , with the negative angle indicating clockwise. Thus φ is roughly -15° .

The final unknown quantity from Fig. 5 is the nadir location n . The reported azimuth angle ϕ gives the angle clockwise from the ground range line g to North. Thus the nadir location is found³ by starting at the center c and moving a distance g in bearing ϕ .

Figure 6 shows the ground geometry to find the ground velocity. The nadir and measurement center points n and c are labeled. The track direction is labeled as t , as is the direction to North. The reported measurement azimuth angle ϕ is the angle from the ground range line to North. From ϕ and the beam layout we compute φ , the angle from the track direction to North. By some geometry this can be shown to be

$$\varphi = \begin{cases} \phi - 135^\circ & \text{beam 1} \\ \phi - 90^\circ & \text{beam 2} \\ \phi - 45^\circ & \text{beam 3} \\ \phi + 135^\circ & \text{beam 4} \\ \phi + 90^\circ & \text{beam 5} \\ \phi + 45^\circ & \text{beam 6} \end{cases} \quad (8)$$

Figure 6 illustrates beam 6. A positive angle rotates in the counter-clockwise direction.

For each grid point (x, y) on the tangent plane, the grid coordinate is converted from northing/easting to latitude and longitude using [6]. The great circle distance between that location and nadir is computed to find $g(x, y)$. The central angle $\alpha(x, y)$ is computed using Eq. (7). The Law of Cosines is used to find the slant range distance $r(x, y)$ for every point on the tangent plane:

$$r(x, y)^2 = R_{sat}^2 + R_E^2 - 2R_ER_{sat} \cos \alpha(x, y). \quad (9)$$

Orbital motion is simulated by shifting the tangent plane coordinates after a time increment δ_t . The ground-track velocity is $v \approx 6.7$ km in the along-track direction. This is converted to the northing/easting coordinate system by rotating the track velocity by $-\varphi$:

$$\begin{bmatrix} dx \\ dy \end{bmatrix} = \begin{bmatrix} \cos(-\varphi) & -\sin(-\varphi) \\ \sin(-\varphi) & \cos(-\varphi) \end{bmatrix} \begin{bmatrix} 0 \\ v\delta_t \end{bmatrix} \quad (10)$$

$$= \begin{bmatrix} v\delta_t \sin \varphi \\ v\delta_t \cos \varphi \end{bmatrix}. \quad (11)$$

³One formula for this is found on <http://www.movable-type.co.uk/scripts/latlong.html>

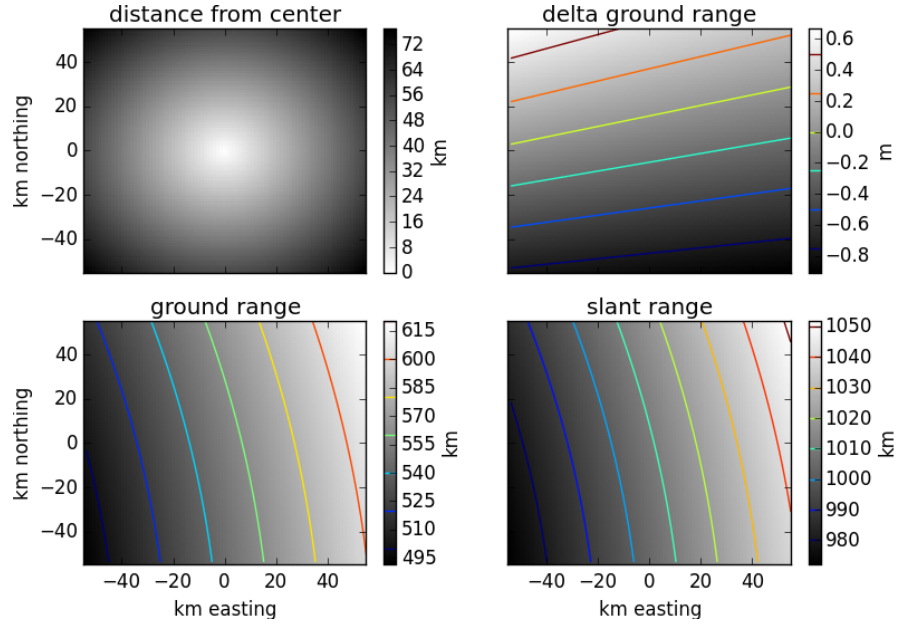


Figure 7: The grid point values for a measurement from a mid beam. Clockwise from upper left: distance from grid center, change in ground range after a time differential, slant range, and ground range.

Earth rotation is simulated by incrementing the x (easting) coordinate:

$$dx' = dx + R_{lat} \omega \delta_t, \quad (12)$$

where $R_{lat} = R_E \cos(\text{lat})$ is the radius of the local latitude line and the rotation rate of the Earth is $\omega = 7.2921150 \times 10^{-5}$ rad/s.

The ground and slant ranges are recomputed after the time increment δ_t . A value of $1 \mu\text{s}$ is used for δ_t . To find the Doppler frequency requires computing the velocity of each grid point in the slant range direction. This is given as

$$v_r(x, y) = \frac{r'_d(x, y) - r_d(x, y)}{\delta_t}, \quad (13)$$

where v_r is the slant range velocity, r_d the slant range, and r'_d the slant range after the time differential δ_t . The range, Doppler, and discriminator frequencies are computed using Eq. (2).

The quantities computed above are shown in the following figures for an actual measurement. The measurement is from the right mid beam, ascending pass, 38.24° incidence angle, 66.52°N 299.67°E , at 2011-10-26 01:00:01.254Z. The distance from grid center, slant range, and ground range are shown in Fig. 7. The range and Doppler frequencies are shown in Fig. 8, and the discriminator frequencies in Fig. 9.

The SRF due to only the on-board processing is dictated by the discriminator frequency and the windowed FFT bin response. The windowed FFT bin response for ASCAT is detailed in Appendix A and is stored in normalized units of FFT bins. The discriminator frequency at each grid point, which is in units of Hz, is converted to units

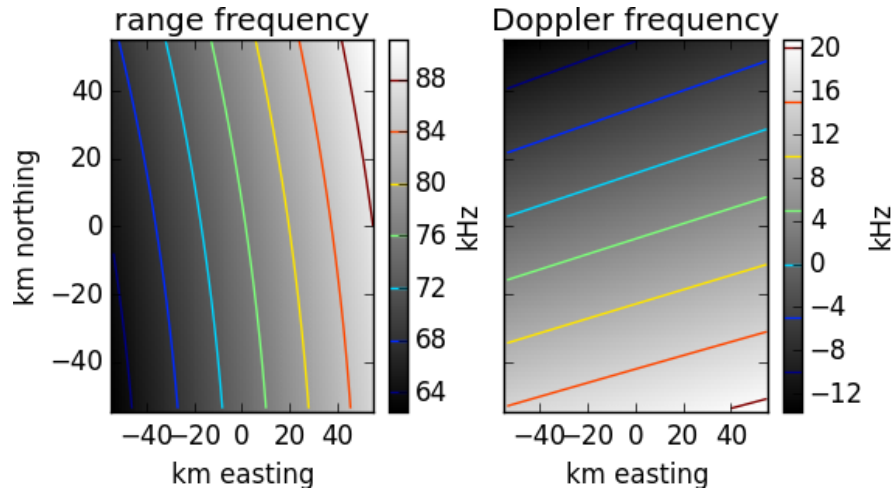


Figure 8: The grid point values for a measurement from a mid beam. The range and Doppler frequencies are shown.

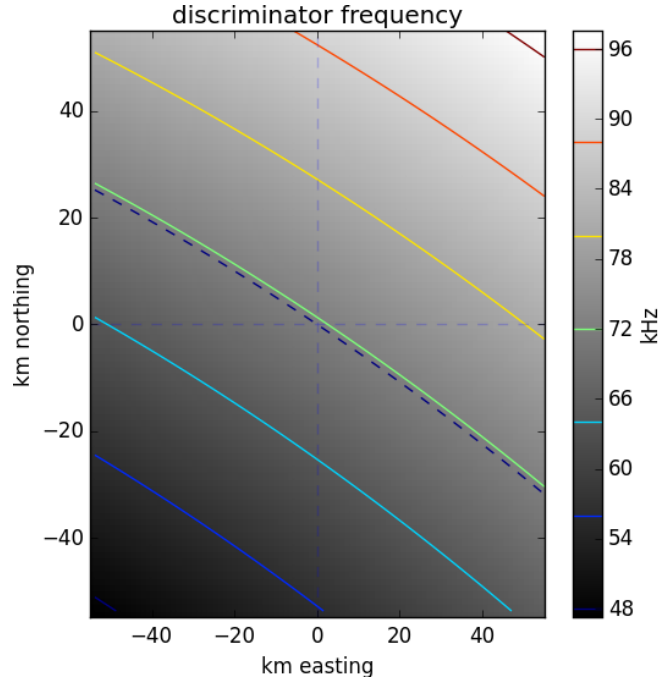


Figure 9: The grid point values for a measurement from a mid beam. The discriminator frequencies are shown.

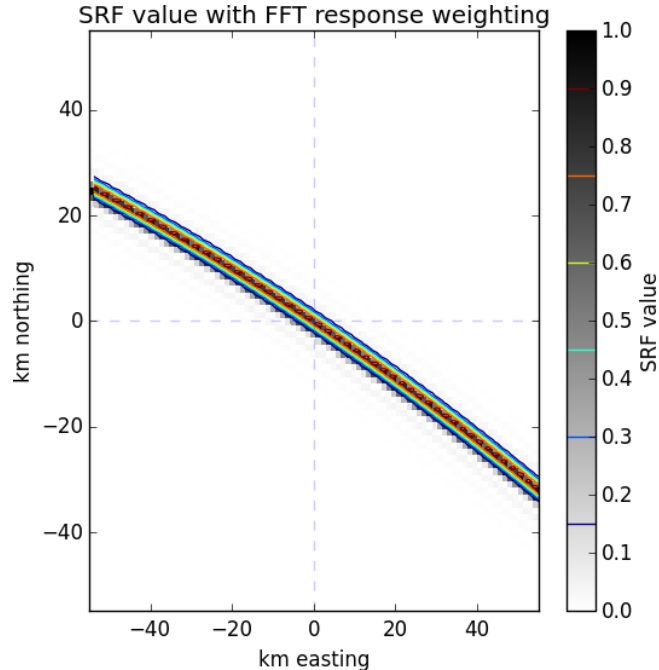


Figure 10: The pulse SRF value due to only the FFT response.

of FFT bins:

$$f_{\text{disc,norm}} = \frac{(f_{\text{disc}} - f_{\text{cen}})\text{Hz}}{412.5 \times 10^3 \text{ Hz}/512 \text{ bins}}, \quad (14)$$

where f_{cen} is the discriminator frequency at the grid center. The offset and scaled discriminator frequency grid is input to the ASCAT windowed FFT bin response from Appendix A.3 to find the processing-only pulse SRF. For the measurement used in Fig. 9, the corresponding FFT response is shown in Fig. 10.

To find the response due to the antenna pattern, only the antenna patterns in the cross-beam direction are used. This assumes that over the SRF the along-beam antenna pattern is constant. To incorporate the two-way gain, the magnitude-square of the normalized antenna gain pattern is used. The patterns differ for the mid and side beams and are shown in Fig. 2. The nominal antenna patterns are provided by [7]. For each grid point, the cross-beam distance from the along-beam line, d_b , is computed. The distance in antenna azimuth from the pattern center, $\Delta\phi$, is computed using some trigonometry:

$$\sin(\Delta\phi) = d_b/s. \quad (15)$$

Figure 11 shows d_b and $\Delta\phi$. The $\Delta\phi$ values are input to the antenna pattern to find the SRF response due to the antenna, shown in Fig. 12.

The pulse SRF is the multiplication of the antenna pattern (Fig. 12) and the FFT response (Fig. 10), shown in Fig. 13.

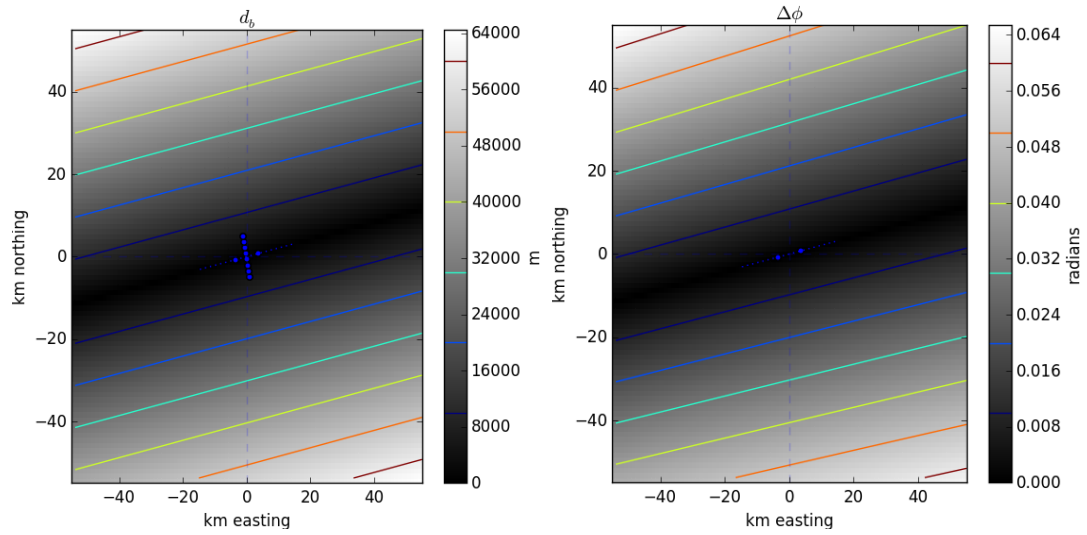


Figure 11: The cross-beam distance (left) and antenna azimuth angle (right).

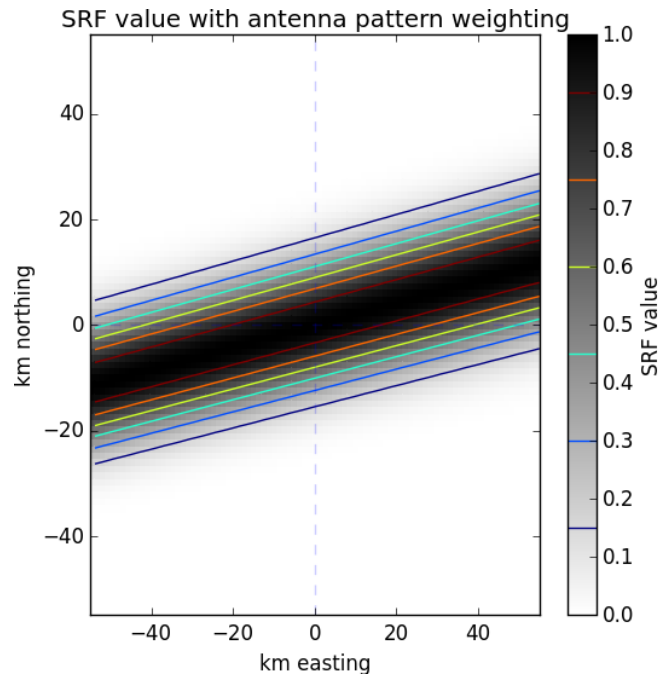


Figure 12: The pulse SRF value due to only the antenna response.

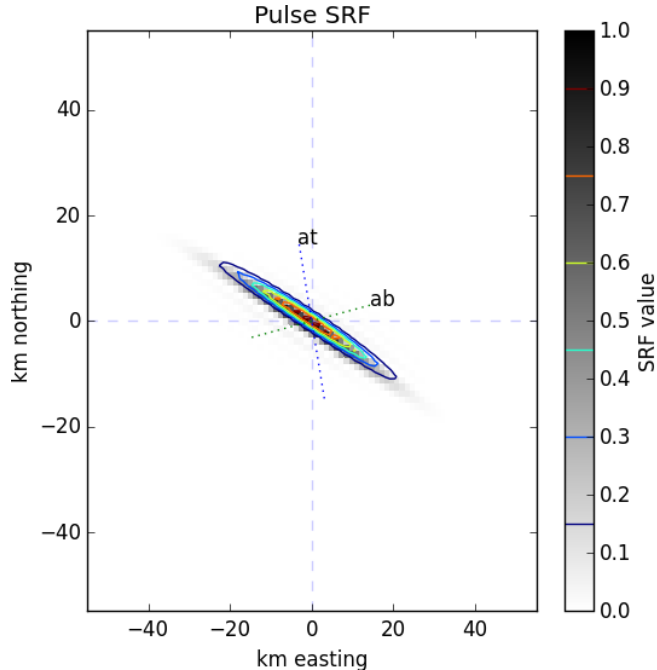


Figure 13: The pulse SRF value. The along-track (“at”) and along-beam (“ab”) directions are indicated.

3.2 Measurement SRF

Each reported measurement is the weighted combination of eight pulses or echoes. Thus, the SRF of a reported measurement is the weighted combination of the SRFs for the pulses. Because of platform motion, the individual pulse SRFs are offset from each other, so the measurement SRF is a “smeared” pulse SRF.

To compute the measurement SRF, the pulse SRF is first estimated. In order for the eight pulse SRFs to be correctly offset (i.e., not limited by the grid spacing), a bivariate spline is fit to the pulse SRF grid point values. The spline is appropriately offset in the along-track direction for each of the eight pulses. The pulse locations are not reported, but are estimated based on the measurement center, the along-track direction, and the ground track velocity of 6.7 km/s. Each measurement SRF grid point value is the weighted combination of the eight pulse SRFs at that grid point.

After combination of eight pulse SRFs, the measurement SRF is illustrated in Fig. 14. Another bivariate spline is fit to the measurement SRF. When the SRF value for an (x, y) location on the tangent plane is requested, the spline is used to evaluate the SRF value at that location.

4 Parameterized SRF Estimate

Computing the SRF estimate and evaluating it for several points for each measurement is a time-consuming process. In order to speed up the SRF estimate, a parameterized version is developed. This both speeds up the processing and simplifies the code required

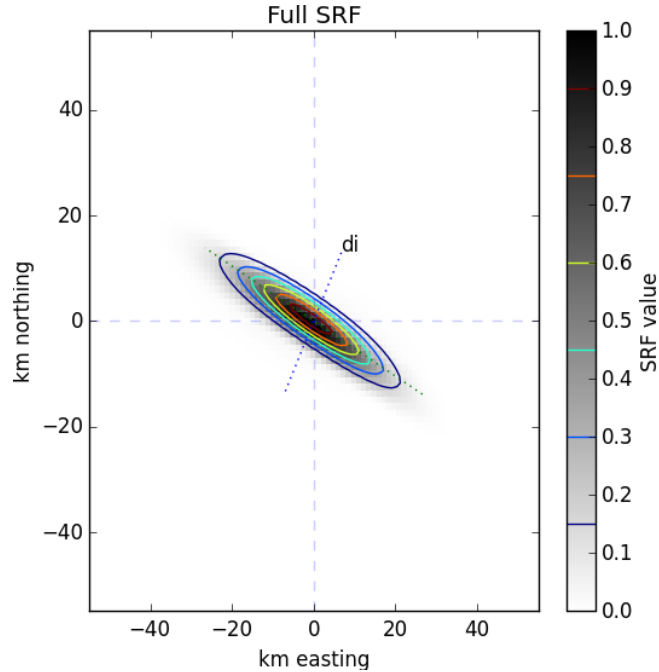


Figure 14: The measurement SRF value.

to implement it.

The parameterization is based on the observation that the measurement SRF estimate is generally an ellipse, rotated such that the semi-minor axis is aligned with the gradient of the discriminator frequency. The rotation angle between the along-beam axis and the discriminator frequency gradient is termed α .

The cumulative rotation angle between northing and the discriminator frequency gradient is:

$$\theta = \alpha + \beta + (-\varphi) \quad (16)$$

where β is the rotation angle between along-beam and cross-track and φ is the rotation angle from along-track to northing. The angle φ is defined in Eq. (8) and β is:

$$\beta = \begin{cases} 45^\circ & \text{beam 1} \\ 90^\circ & \text{beam 2} \\ 135^\circ & \text{beam 3} \\ -45^\circ & \text{beam 4} \\ -90^\circ & \text{beam 5} \\ -135^\circ & \text{beam 6} \end{cases} . \quad (17)$$

The geometry for these rotation angles is shown in Fig. 15, illustrating the case for beam 1. The cumulative angle θ describes the rotation from northing to the semi-minor ellipse axis. The ellipse axes are labeled x and y , with angle α describing the rotation between the ellipse and the along-beam direction.

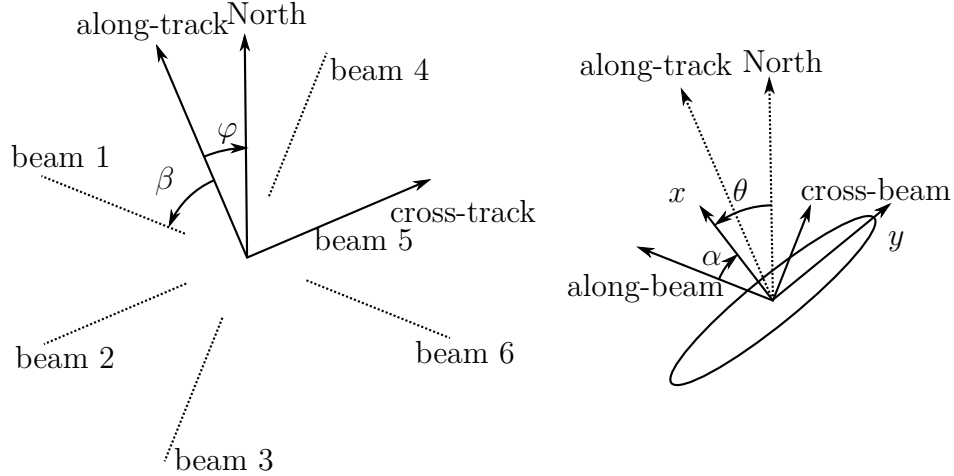


Figure 15: Left: the rotation angles φ and β for beam 1. Right: the rotation angles α and θ for beam 1.

The SRF is treated as separable in the x and y directions aligned with the ellipse. With the above geometry, three parameters are modeled: (1) the rotation angle θ , (2) the SRF response along the x axis, and (3) the SRF response along the y axis. To compute the SRF value for a location near a measurement, the following high-level algorithm is used:

1. Define a location on the locally tangent plane centered on the measurement
2. Convert from tangent plane coordinates $(x_{\text{tp}}, y_{\text{tp}})$ to coordinates with respect to the SRF ellipse (x_d, y_d) using the rotation angle θ
3. Look up the SRF response in the x direction
4. Look up the SRF response in the y direction
5. Multiply the x and y response values together to obtain the SRF value

The angle θ is found directly in the full estimate by finding the gradient of the computed discriminator frequencies on the tangent plane grid. However, rather than parameterizing the angle θ , the angle α is parameterized instead. This is due to the difficulty in fitting θ at high latitudes due to the rapidly varying azimuth angle. The remaining components of θ — β and φ —are only a function of the beam number and azimuth angle so are not parameterized.

The angle α is found to follow a surface as a function of measurement node and latitude. An example is shown in Fig. 16. A fourth-order polynomial surface is fit separately for the six beams, also separated into ascending and descending passes. Thus the α parameterization is:

$$\alpha(n, l; b, a) = c_{00} + c_{01}n + c_{02}n^2 + \dots + c_{10}l + c_{11}nl + \dots + c_{44}n^4l^4 \quad (18)$$

where n is the node number, l the latitude, b the beam number and a is ascending or descending. For each combination of b and a , $(4 + 1)^2 = 25$ coefficients are found. With

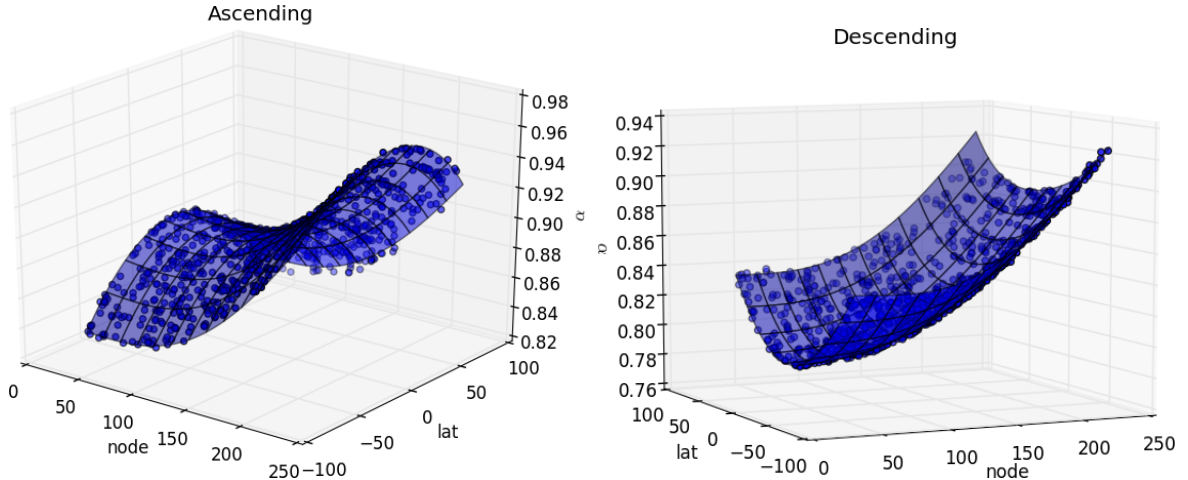


Figure 16: The angle α , in radians, is shown as a function of node and latitude for beam 6 for both ascending and descending passes. The points are a random sample chosen from 5 days of ASCAT data. The surface, a fourth-order polynomial, is fit to the points.

six beams ($b \in \{1, \dots, 6\}$) and two cases for ascending/descending ($a \in \{0, 1\}$), there are twelve sets of coefficients.

The coefficients are determined by computing the full SRF estimate for a large number of ASCAT measurements, randomly distributed in latitude and node. For about 190 000 measurements per combination of beam and ascending/descending, the R^2 coefficient of determination is above 0.99 in all cases. R^2 is a metric that describes the goodness of fit and ranges between 0 and 1. Such a high value indicates that the polynomial model chosen nearly perfectly describes the data.

For the SRF response values, the approximation chosen here models the SRF mainlobe using a polynomial fit. In dB space, a polynomial fits better to the response without requiring a high-order polynomial. This is due to the “tail” in linear space that is difficult to fit to a low-order polynomial. A sample SRF response and the polynomial fit are shown in Fig. 17.

The polynomial fit is constrained so it only fits the mainlobe down to -15 dB. This is to avoid fitting the “ripples” in the mainlobe (which would require a higher-order polynomial) and because the SRF estimate is only needed for the mainlobe down to about -10 dB. A biquadratic fit is applied, or a fourth-order polynomial fit with the odd terms set to 0:

$$\text{SRF}_x(x; \dots) = a_0 + a_2x^2 + a_4x^4 \quad (19)$$

$$\text{SRF}_y(y; \dots) = b_0 + b_2y^2 + b_4y^4 \quad (20)$$

This odd terms are set to 0 to enforce symmetry. x and y are in units of km from the center of the locally tangent plane.

Equations (19) and (20) are for a specific SRF. To cover the general case, the coefficients are, as with the angle α , functions of node, latitude, beam, and ascending/descending pass. A polynomial surface is fit to each coefficients as a function of node and latitude. However, unlike for α , only a second-order polynomial surface is

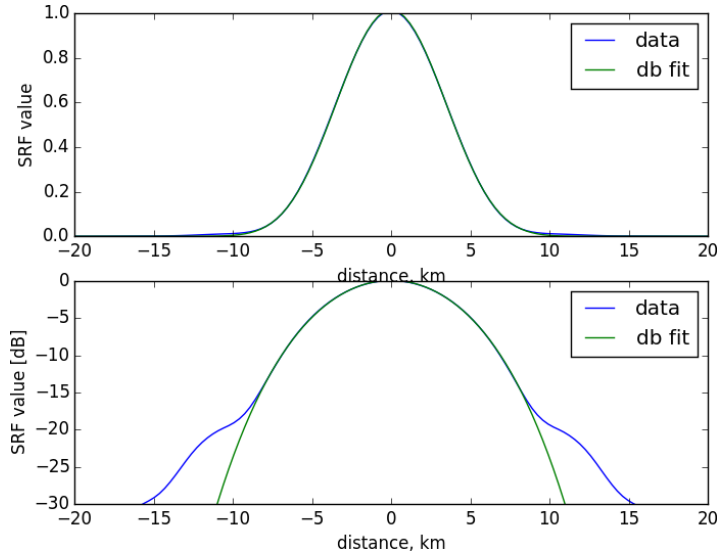


Figure 17: The SRF values along the x axis for a measurement from beam 3. The upper subplot shows the values in linear space, the lower subplot shows the values in dB space. A biquadratic fit in dB space is applied to the data down to -15 dB.

required. For example, for the a_0 coefficient from Eq. (19):

$$a_0(n, l; b, a) = a_{00} + a_{01}n + a_{02}n^2 + a_{10}l + a_{11}nl + \dots + a_{22}n^2l^2 \quad (21)$$

For each of the six coefficients from Eqs. (19) and (20), there are $(2 + 1)^2 = 9$ coefficients. As with α , the fits are separately performed by beam and ascending/descending pass, for twelve cases. Thus $6 \times 9 \times 12 = 648$ coefficients are used to parameterize the SRF response.

5 Results

Both the full and parameterized SRF estimates are implemented in C. The spline fitting portions of the full estimate use the DFITPACK⁴ Fortran library. Both implementations contain the same public function names. On the same computer, these functions are benchmarked, with the mean and standard deviation timing per function call shown in Table 2.

The `srf_init` and `srf_done` functions are called once each before and after using the SRF library. The `srf_meas` and `srf_free` functions are called once per measurement. The `srf_latlon_extent` function is optional but would be called only once per measurement. The `srf_eval_ll` and `srf_eval_xy` functions are typically called many times per measurement. In order to estimate the expected SRF computation time per measurement, the timings for one call each of `srf_meas`, `srf_latlon_extent`, and `srf_free` are added together. A conservative estimate is $10^2 = 100$ calls of `srf_eval_ll` per measurement, so this is also added to the measurement time.

⁴<http://www.netlib.org/dierckx/>

Table 2: The mean and standard deviation function timing per run for the full and parameterized SRF estimate implementations. The expected measurement time is based on 100 calls to `srf_eval_ll` and one call each to `srf_latlon_extent`, `srf_meas`, and `srf_free`.

| Function | Full, μ s | Parameterized, μ s |
|--------------------------------|---------------------|------------------------|
| <code>srf_init/srf_done</code> | 388.10 ± 42.04 | 0.5562 ± 0.9708 |
| <code>srf_meas/srf_free</code> | $19\,430 \pm 3353$ | 5.776 ± 9.747 |
| <code>srf_latlon_extent</code> | 130.700 ± 4.305 | 2.5240 ± 0.9347 |
| <code>srf_eval_ll</code> | 0.5547 ± 0.2692 | 0.9651 ± 0.5879 |
| <code>srf_eval_xy</code> | 0.3850 ± 0.2308 | 0.1954 ± 0.3068 |
| Expected meas time | 19.61 ms | 0.1048 ms |

From examining the function timings in Table 2, the parameterized estimate is two orders of magnitude faster to complete than the full estimate. Most of the slowdown in the full estimate is in the `srf_meas` function, which creates the grid on the locally tangent plane and computes the discriminator frequency and eventually the SRF value for each grid point. Since the parameterized version merely performs a few polynomial evaluations, it is much faster to complete.

Comparison plots for the full and parameterized SRF estimates are shown in Figs. 18 and 19 for a side and mid beam, respectively. The estimated SRF values are very similar for the two estimates. The largest differences are for measurements with low incidence angles in the mid beams. In these cases, the full SRF curves slightly, deviating from the ellipse model. The parameterized SRF does not account for the curvature. Since the difference is small, and in the interest of a simple and quick parameterized estimate, the curvature is not accounted for.

6 Conclusion

Two estimates of the spatial response function for each ASCAT measurement are developed in this report. The full estimate defines a grid of points on a locally tangent plane to the measurement center and computes intermediate SRF quantities such as the discriminator frequency. The nominal antenna pattern and the windowed FFT bin response are used to compute the SRF for each pulse. Along-track pulse averaging is accounted for, resulting in a bivariate spline that is fit to the measurement SRF.

Since this is a computationally intensive process, a parameterized SRF is also developed. The SRF is modeled as separable and a two-layer polynomial fit is used to compute the SRF values. The appropriate rotation angle is also modeled. The parameterized SRF takes as input the node number, beam, latitude, and the ascending/descending pass indicator.

The two SRF estimates are benchmarked and the parameterized SRF is found to be two orders of magnitude faster to compute per measurement. While it does not exactly represent the full estimate, it is a close approximation, more than necessary for enhanced resolution processing or to compute the measurement land fraction (either

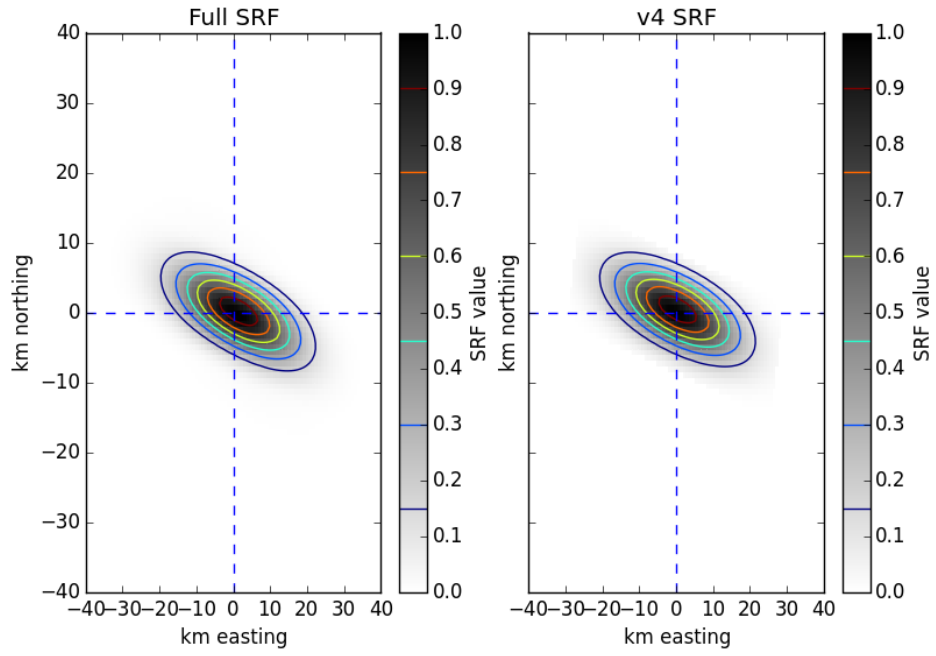


Figure 18: The full (left) and parameterized (right) SRF estimates for beam 6.

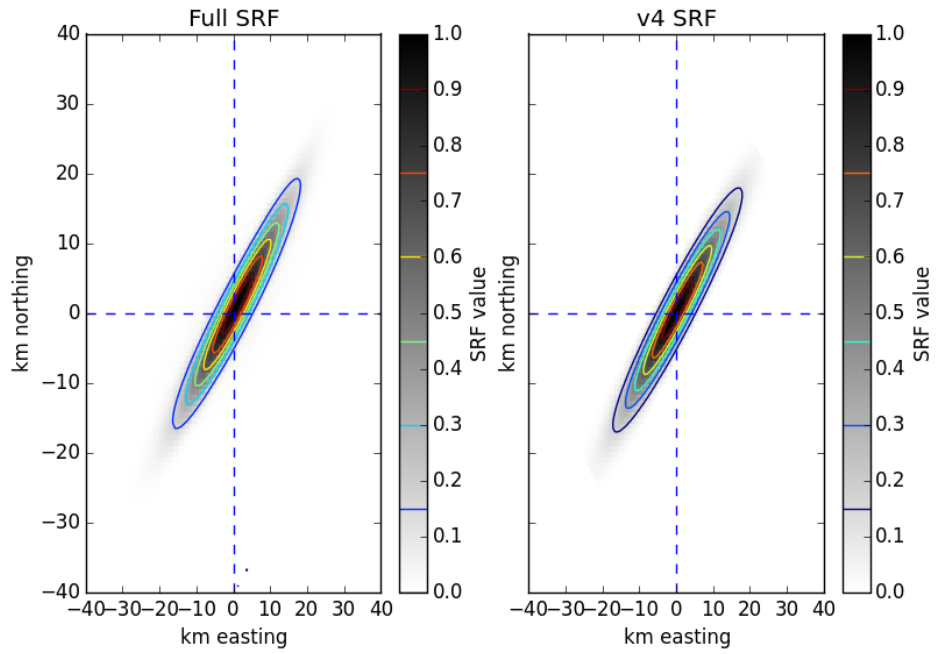


Figure 19: The full (left) and parameterized (right) SRF estimates for beam 2.

case requires a spatial resolution of only a few km). Thus the parameterized estimate is preferred for operational purposes, but the full estimate is useful for research purposes.

Acknowledgment

I am grateful for the assistance of Craig Anderson, Julia Figa, and Julian Wilson, of EUMETSAT. The technical information provided about ASCAT, its on-board processing, and the ground processing is invaluable to the development of an accurate measurement spatial response function.

References

- [1] J. Figa-Saldaña, J. J. W. Wilson, E. Attema, R. Gelsthorpe, M. R. Drinkwater, and A. Stoffelen, “The advanced scatterometer (ASCAT) on the meteorological operational (MetOp) platform: A follow on for European wind scatterometers,” *Canadian Journal of Remote Sensing*, vol. 28, no. 3, pp. 404–412, 2002. [Online]. Available: <http://pubs.casi.ca/doi/abs/10.5589/m02-035>
- [2] *ASCAT Level 1: Product Format Specification*. EUMETSAT, 17 March 2014, no. EPS.MIS.SPE.97233. [Online]. Available: http://www.eumetsat.int/website/wcm/idc/idcplg?IdcService=GET_FILE&dDocName=PDF_TEN_97233-EPS-ASCAT-L1&RevisionSelectionMethod=LatestReleased&Rendition=Web
- [3] *ASCAT Product Generation Function Specification*, 2005. [Online]. Available: http://eumeds.eumetsat.int/groups/ops/documents/document/PDF_TEN_990009-EPS-ASCAT-PGS.pdf
- [4] C. Anderson, H. Bonekamp, C. Duff, J. Figa-Saldana, and J. J. W. Wilson, “Analysis of ASCAT ocean backscatter measurement noise,” *Geoscience and Remote Sensing, IEEE Transactions on*, vol. 50, no. 7, pp. 2449–2457, July 2012.
- [5] J. J. W. Wilson, C. Anderson, M. A. Baker, H. Bonekamp, J. Saldaña, R. G. Dyer, J. A. Lerch, G. Kayal, R. V. Gelsthorpe, M. Brown, E. Schied, S. Schutz-Munz, F. Rostan, E. W. Pritchard, N. G. Wright, D. King, and U. Onel, “Radiometric calibration of the advanced wind scatterometer radar ASCAT carried onboard the METOP-A satellite,” *Geoscience and Remote Sensing, IEEE Transactions on*, vol. 48, no. 8, pp. 3236–3255, Aug 2010.
- [6] I. S. Ashcraft, “Projecting an Arbitrary Latitude and Longitude onto a Tangent Plane,” BYU MERS Technical Report #99-04, Tech. Rep., 1999. [Online]. Available: <http://www.mers.byu.edu/docs/reports/MERS9904.pdf>
- [7] J. J. W. Wilson, “ASCAT inverse impulse response function,” Personal communication (email), Jan 2009.

- [8] A. V. Oppenheim, R. W. Schaffer, and J. R. Buck, *Discrete-Time Signal Processing*, 2nd ed. Prentice Hall, 1998.

A ASCAT FFT Bin Response

The FFT (fast Fourier transform), being a DFT (discrete Fourier transform), is the sampled version of the DTFT (discrete-time Fourier transform). The number of FFT bins is the number of samples from the DTFT. The frequency response of an FFT bin is computed in Appendix A.1. This uses a rectangular window. The ASCAT window is described in Appendix A.2 and the corresponding FFT bin response in Appendix A.3.

A.1 Rect window response

For the discrete-time signal⁵ $x[n]$ with length N (and assumed to be periodic with period N), the DTFT is expressed as

$$X(e^{j\omega}) = \sum_{n=0}^{N-1} x[n]e^{-j\omega n}. \quad (22)$$

The DFT is

$$X[k] = \sum_{n=0}^{N-1} x[n]e^{-j2\pi kn/N} \quad (23)$$

$$= X(e^{j\omega})|_{\omega=2\pi k/N}. \quad (24)$$

Implicit in these definitions is a window function, $w[n]$, so that $x[n]$ is replaced with $x[n]w[n]$. The response of an FFT bin depends on the window used. Due to the convolution theorem,

$$\text{DTFT}\{x[n]w[n]\} = X(e^{j\omega}) * W(e^{j\omega}). \quad (25)$$

We evaluate $W(e^{j\omega})$ for a rect⁶ window (or, an implicit window), so that $w[n] = 1$ for all n . The DTFT of $w[n]$ is then

$$W(e^{j\omega}) = \sum_{n=0}^{N-1} e^{-j\omega n} = \frac{1 - e^{-j\omega N}}{1 - e^{-j\omega}}. \quad (26)$$

Making use of the following expansions:

$$1 - e^{-j\omega} = e^{-j\omega/2}(e^{j\omega/2} - e^{-j\omega/2}) \quad (27)$$

$$1 - e^{-j\omega N} = e^{-j\omega N/2}(e^{j\omega N/2} - e^{-j\omega N/2}), \quad (28)$$

then the DTFT of a rect can be written as:

$$W(e^{j\omega}) = \frac{1 - e^{-j\omega N}}{1 - e^{-j\omega}} = \frac{e^{-j\omega N/2}}{e^{-j\omega/2}} \left(\frac{e^{j\omega N/2} - e^{-j\omega N/2}}{e^{j\omega/2} - e^{-j\omega/2}} \right) \frac{2j}{2j} \quad (29)$$

$$= e^{-j\omega(N-1)/2} \frac{\sin(\omega N/2)}{\sin(\omega/2)}. \quad (30)$$

⁵This is using notation from [8].

⁶A rect window is the rectangular window, or a window with a value of 1 for some domain, and 0 elsewhere.

Recalling that one definition of the Dirichlet kernel (or “periodic sinc” function) is

$$D_n(x) = \frac{\sin(nx/2)}{\sin(x/2)}, \quad (31)$$

then the DTFT is expressed in terms of the Dirichlet kernel,

$$W(e^{j\omega}) = e^{-j\omega(N-1)/2} D_N(\omega). \quad (32)$$

Since we are interested in the power spectrum, the magnitude-squared response is

$$|W(e^{j\omega})|^2 = |D_N(\omega)|^2. \quad (33)$$

This result is the continuous-valued frequency response of a rect window function, using a DTFT. In practice, a DTFT is approximated by a DFT with sufficiently many samples. Thus, while Eq. (33) gives the analytic frequency response of an FFT bin, it could also be computed by zero-padding the rect window $w[n]$ by some amount and then computing the FFT.

Since the signal spectrum $X(e^{j\omega})$ is convolved with the window spectrum $W(e^{j\omega})$, the value of a given FFT bin is not the sample of only the signal, but the linear combination of all signal frequencies weighted by the window spectrum.

Some examples are shown in Fig. 20. The frequency response for a 16-point FFT is shown. The frequencies for FFT bin centers are indicated with the stem plots. Note that the response follows a Dirichlet kernel. Additionally, the frequency response of any given bin is the weighted combination of all other frequencies except for the frequencies at the centers of the other bins.

A.2 ASCAT on-board processing

ASCAT transmits linear FM pulses⁷. The received signal is dechirped and sampled at 412.5 kHz. The sampled mid and side beams contain 2252 and 3193 samples, respectively. These samples are then divided into overlapping chunks of 512 samples. Each FFT chunk is referred to as a *range look*.

The window applied to each chunk is specified in [3], Eq. 6.2.7-8. The number of chunks and the window parameters are shown in Table 3. Each chunk is windowed, then a 512 point FFT is performed. Half of the samples are discarded (the negative frequencies are redundant in a real-valued signal) and the magnitude-square is taken. All the transformed chunks are averaged together to give the final power spectrum estimate, power vs frequency, which maps to σ° vs range.

The window function is described as

$$w(t) = \begin{cases} c & 0 \leq |t| \leq pT_{rl}/2 \\ \frac{c}{2} \left[1 + \cos\left(\frac{2\pi(|t|-pT_{rl}/2)}{T_{rl}(1-p)}\right) \right] & pT_{rl}/2 \leq |t| \leq T_{rl}/2 \end{cases}, \quad (34)$$

where T_{rl} is the “range look duration” and is 1.241 212 ms. Note that c and p differ for mid and side beams. The sampled window function $w[n]$ is $w(t)$ where $t \in [-T_{rl}/2, T_{rl}/2]$ and $N = 512$ samples are taken. The window function is plotted in Fig. 21 for the mid and side beams. The window is a tapered rect, similar to a Tukey window.

⁷Most of the information in this section comes from [7], an email from Julian Wilson on 2009-01-23.

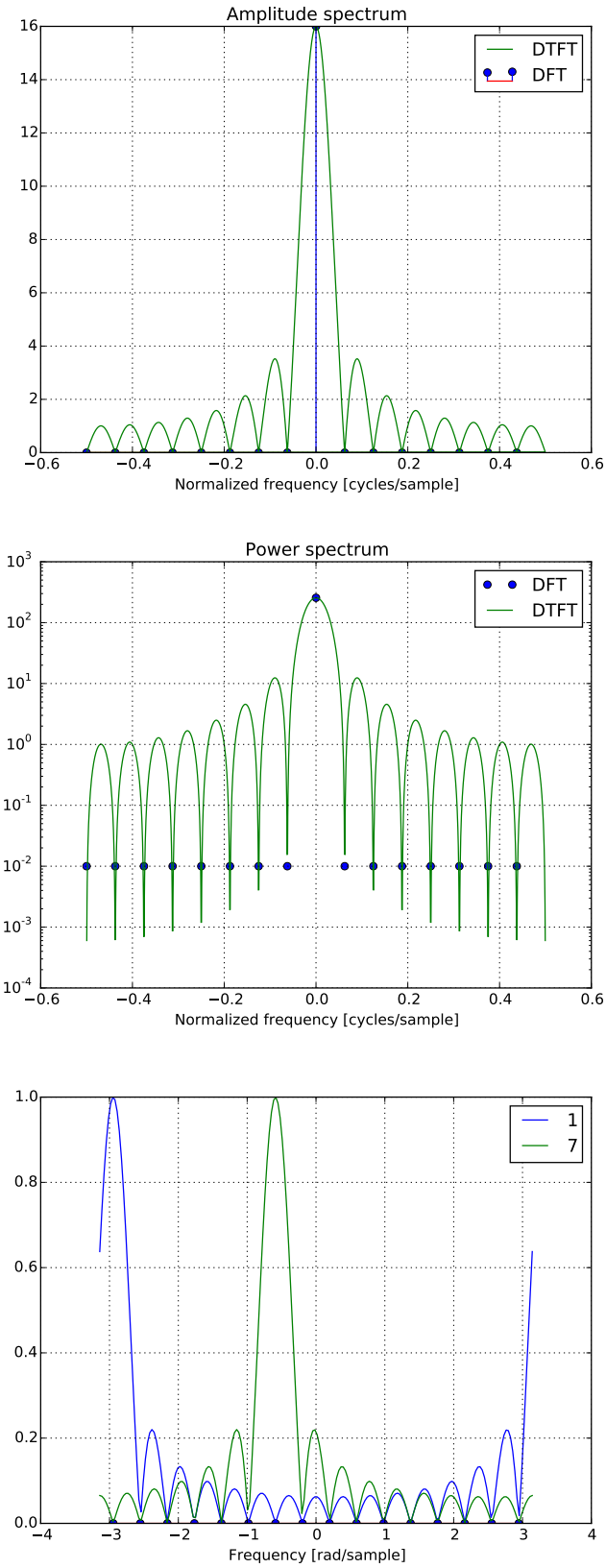


Figure 20: The magnitude (top) and magnitude-squared (middle) frequency response of an FFT bin. The frequency response (bottom) for two sample bins in a 16-point FFT.

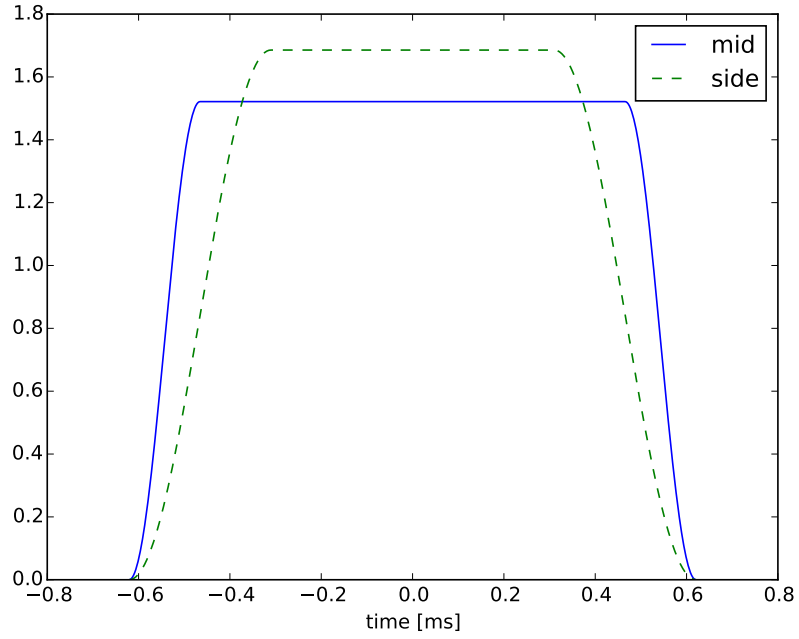


Figure 21: The window function applied to each 512-sample chunk.

Table 3: FFT chunk parameters

| Beam | FFT chunks | Chunk window parameters |
|------|------------|--------------------------|
| Mid | 5 | $c=1.521\ 45$, $p=0.75$ |
| Side | 8 | $c=1.685\ 56$, $p=0.5$ |

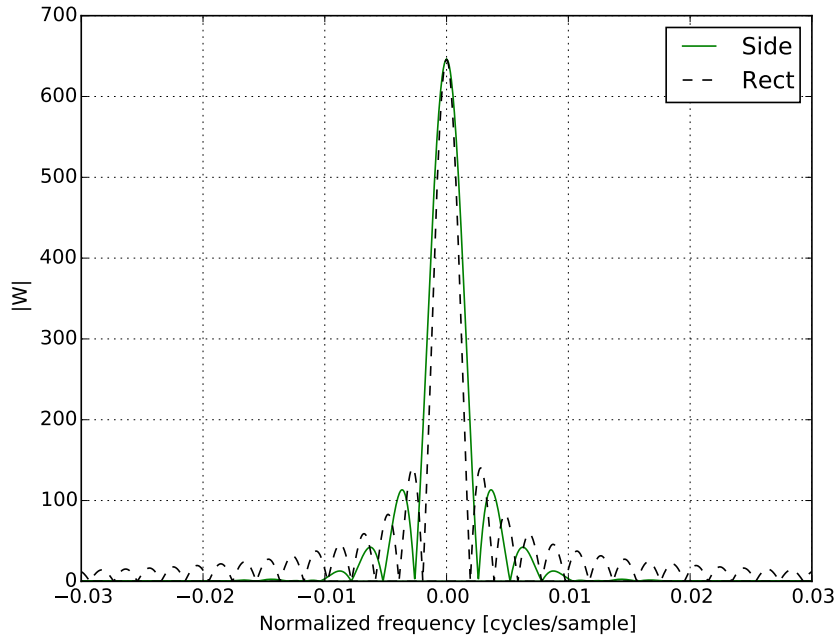


Figure 22: The magnitude of the Fourier transform of the chunk window for side beams, along with the response from a rect window. The rect response has been renormalized to match the peak level of the side range look window response. This plot is horizontally zoomed in order to show more detail near the mainlobe (the full domain is -0.5 to 0.5 cycles/sample).

A.3 Windowed FFT bin response

The magnitude of the Fourier transform for one of the windows is shown in Fig. 22, with the response from a rect window, for comparison. While the peak sidelobe level and mainlobe width are not drastically different from the rect response, the sidelobes taper off more quickly. As shown in Fig. 23, the mainlobe width for the windows is only slightly wider than the rect window.

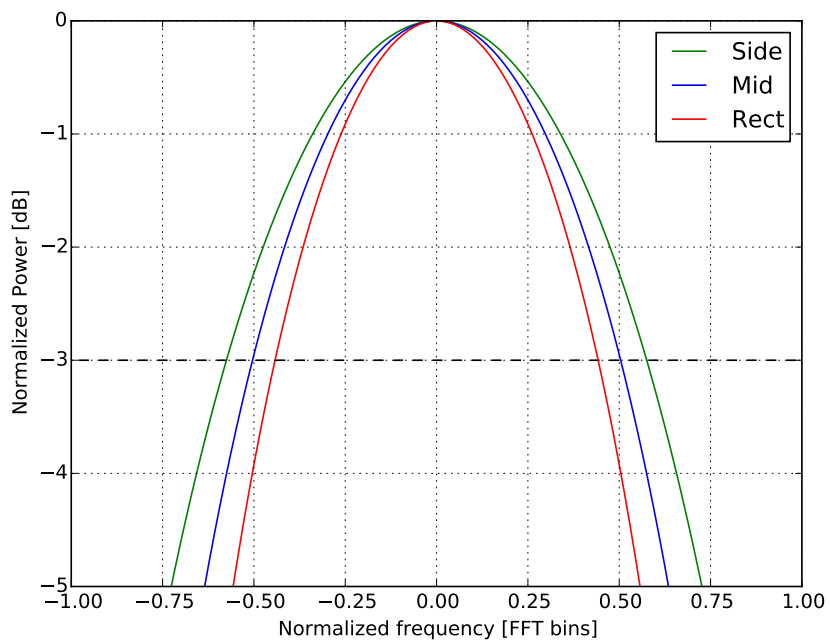


Figure 23: The magnitude-squared of the Fourier transform of the chunk windows, along with a rect window for comparison. This plot is horizontally zoomed in order to show more detail near the mainlobe. The 3 dB width of the windows is estimated to be 0.88, 1.0, and 1.125 FFT bins for the rect, mid, and side windows, respectively.